Optimizing Interface Conductivity in Electronics

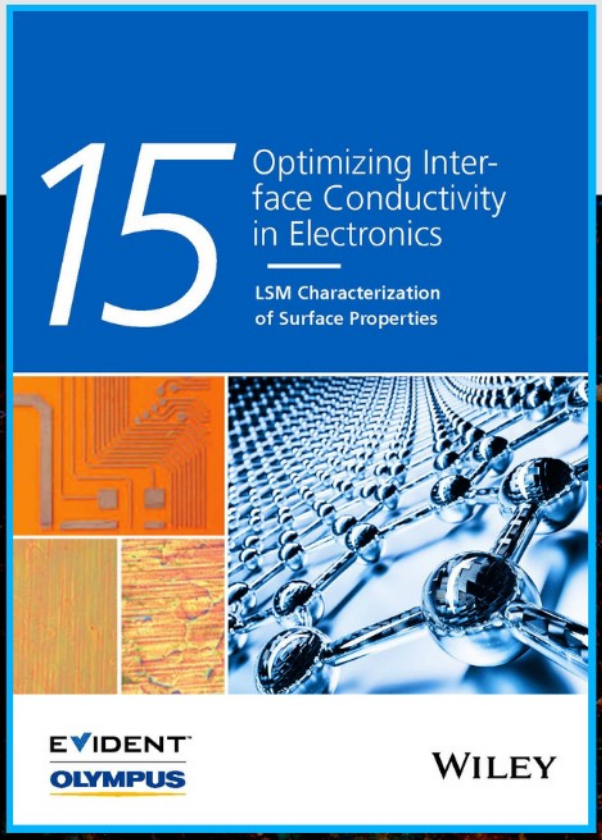

The latest eBook from Advanced Optical Metrology. Download for free.

Surface roughness is a key parameter for judging the performance of a given material's surface quality for its electronic application. A powerful tool to measure surface roughness is 3D laser scanning confocal microscopy (LSM), which will allow you to assess roughness and compare production and finishing methods, and improve these methods based on mathematical models.

Focus on creating high-conductivity electronic devices with minimal power loss using laser scanning microscopy is an effective tool to discern a variety of roughness parameters.

EVIDENT
OLYMPUS

WILEY

Check for updates

ADVANCED FUNCTIONAL MATERIALS
www.afm-journal.de

Rational Design of Covalent Multiheme Cytochrome-Carbon Dot Biohybrids for Photoinduced Electron Transfer

Huijie Zhang, Carla Casadevall, Jessica H. van Wonderen, Lin Su, Julea N. Butt, Erwin Reisner,* and Lars J. C. Jeuken**

Biohybrid systems can combine inorganic light-harvesting materials and whole-cell biocatalysts to utilize solar energy for the production of chemicals and fuels. Whole-cell biocatalysts have an intrinsic self-repair ability and are able to produce a wide variety of multicarbon chemicals in a sustainable way with metabolic engineering. Current whole-cell biohybrid systems have a yet undefined electron transfer pathway between the light-absorber and metabolic enzymes, limiting rational design. To enable engineering of efficient electron transfer pathways, covalent biohybrids consisting of graphitic nitrogen doped carbon dots (g-N-CDs) and the outer-membrane decaheme protein, MtrC from *Shewanella oneidensis* MR-1 are developed. MtrC is a subunit of the MtrCAB protein complex, which provides a direct conduit for bidirectional electron exchange across the bacterial outer membrane. The g-N-CDs are functionalized with a maleimide moiety by either carbodiimide chemistry or acyl chloride activation and coupled to a surface-exposed cysteine of a Y657C MtrC mutant. MtrC∼g-N-CD biohybrids are characterized by native and denaturing gel electrophoresis, chromatography, microscopy, and fluorescence lifetime spectroscopy. In the presence of a sacrificial electron donor, visible light irradiation of the MtrC∼g-N-CD biohybrids results in reduced MtrC. The biohybrids may find application in photoinduced transmembrane electron transfer in *S. oneidensis* MR-1 for chemical synthesis in the future.

1. Introduction

In the quest to find alternative sustainable technologies to decrease our reliance on fossil fuels, semiartificial photosynthesis has attracted increasing attention to harvest solar energy for fuel generation.[1] An emerging direction in semiartificial photosynthesis is to interface synthetic, inorganic light-harvesting materials with biocatalysts.[2] Biocatalysts display high selectivity and low overpotential requirements for redox reactions, whereas synthetic nanomaterials offer robust, tunable, and efficient light harvesting properties. Thus, semiartificial photosynthetic systems that combine the advantages of synthetic and biological systems show great promise to overcome the limitations of natural and artificial photosynthesis for the production of solar fuels and added-value chemicals.[1,3]

Inorganic-biological biohybrid systems can be divided into enzyme-based and whole-cell-based systems. Several biohybrid systems combining synthetic light-harvesting materials with enzymes or whole cells have been reported for light-driven reactions,[4] such as H_2 evolution,[5] CO_2 reduction,[6] carbon–carbon bond formation,[7] and N_2 reduction.[8] In enzyme-based biohybrid systems, sacrificial electron donors are typically required to lower charge recombination or back reactions for solar chemicals and fuels generation.[9] In natural photosynthesis, chemical back reactions are further minimized by separating the oxidative and reductive half reactions on either side of the thylakoid membrane.[10] Using whole cells as biocatalysts could mimic such compartmentalization and separate the oxidative reaction at the nanoparticle from the reductive reactions inside the whole-cell biocatalysts. Moreover, living whole-cell biocatalysts can self-replicate, self-repair, and produce

H. Zhang, L. J. C. Jeuken
Leiden Institute of Chemistry
Leiden University
PO Box 9502, Leiden 2300 RA, The Netherlands
E-mail: L.J.C.Jeuken@lic.leidenuniv.nl

The ORCID identification number(s) for the author(s) of this article can be found under https://doi.org/10.1002/adfm.202302204

© 2023 The Authors. Advanced Functional Materials published by Wiley-VCH GmbH. This is an open access article under the terms of the Creative Commons Attribution License, which permits use, distribution and reproduction in any medium, provided the original work is properly cited.

DOI: 10.1002/adfm.202302204

C. Casadevall, L. Su, E. Reisner
Yusuf Hamied Department of Chemistry
University of Cambridge
Lensfield Road, Cambridge CB2 1EW, UK
E-mail: reisner@ch.cam.ac.uk

J. H. van Wonderen, J. N. Butt
School of Chemistry and School of Biological Sciences
University of East Anglia
Norwich Research Park, Norwich NR4 7TJ, UK
E-mail: j.butt@uea.ac.uk

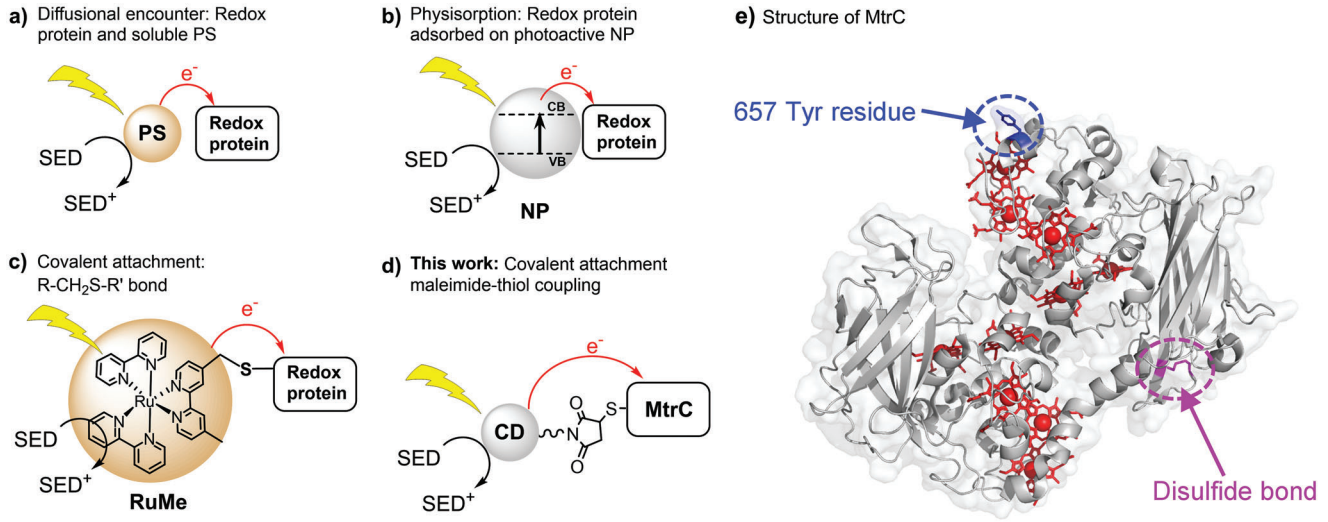

Figure 1. Schematic representation of strategies for photoreduction of *S. oneidensis* MR-1 cytochromes: a) Diffusional encounter: redox proteins and soluble synthetic photosensitizers (PS).[16a,17a] b) Physisorption: redox protein adsorbed on photoactive nanoparticle (NP) (including dye-sensitized TiO_2 nanoparticle).[17a-c] c) Covalent labeling: Redox protein photosensitized by site-selective labeling with [Ru(II)(4-bromomethyl-4′-methylbipyridine)(bipyridine)$_2$]$^{2+}$ (RuMe).[18b] d) This work: Covalent labeling: MtrC photosensitized by site-selective labeling with maleimide functionalized g-N-CD. e) The structure of MtrC. The 10 hemes are in red color. The disulfide bond is shown in magenta. The 657 Tyr (blue) in WT MtrC is mutated to surface exposed Cys (Y657C MtrC). SED: sacrificial electron donor. CB: conduction band. VB: valence band.

complex chemical products due to their diverse metabolic pathways.[1,2,3b,11]

As a model dissimilatory metal-reducing bacterium, *Shewanella oneidensis* MR-1 is a promising biohybrid system as it efficiently exchanges electrons between the cellular metabolism and its external environment.[12] We have previously shown that *S. oneidensis* MR-1 can photocatalytically produce hydrogen and hydrogenate C=C and C=O bonds with soluble organic and inorganic photosensitizers.[12c] However, the products were detected only in the presence of a cell-permeable electron mediator and occurred independently of the metal-reducing (Mtr) pathways responsible for extracellular electron transport. Biohybrid systems with self-assembled CdS nanoparticles on *S. oneidensis* MR-1 have shown light-driven hydrogen generation,[12d] but the complexity of these whole-cell biohybrid systems makes it difficult to differentiate between various electron transfer pathways. It is unclear whether the hydrogen was produced directly by light-harvesting nanoparticles themselves, by nanoparticle-hydrogenase hybrids, or by electron transfer from the nanoparticles through the outer membrane to hydrogenases inside the bacteria. Recent studies on a hybrid system interfacing the CO_2- and N_2-fixing bacterium *Xanthobacter autotrophicus* with CdTe quantum dots show light-driven CO_2 and N_2 fixation with internal quantum efficiencies reaching the biochemical limits. However, the electron transfer pathways from the quantum dots to the microorganism remain unclear.[13] Therefore, rational design of biohybrids is essential to ensure well-defined and effective transmembrane electron transfer and engineer whole-cell biohybrid photocatalysts.

Key to the ability of extracellular electron transfer in *S. oneidensis* MR-1 is a heterotrimeric protein complex, MtrCAB, which provides a direct conduit for bidirectional electron exchange across its outer membrane.[14] Spanning the lipid bilayer is the MtrAB subcomplex with a β-barrel porin (MtrB) wrapped around a decaheme cytochrome (MtrA). Binding the external face of the MtrAB is MtrC, also containing 10 hemes.[15] The combined 20 hemes of MtrCAB create a 185 Å conducting wire that has been shown in vitro to stabilize charge separation of photosensitizer by transferring electrons through the lipid bilayer of a liposome to generate reductive equivalents in the lumen.[16] It has previously been shown that, in the presence of a sacrificial electron donor, MtrC can be photoreduced in vitro by a number of abiotic photosensitizers including dyes and dye-sensitized TiO_2 nanoparticles either in solution or on an electrode.[16a,17] Recently, a Ru(II)(2,2′-bipyridine)$_3$-based dye was covalently attached to MtrC and photoreduction of the 10 heme groups in MtrC was achieved in presence of an electron donor.[18] The state-of-the-art strategies used for the photoreduction of redox proteins, including MtrC, can be summarized as follows: i) Diffusional encounter between redox proteins and soluble synthetic photosensitizers;[16a,17a] ii) Physisorption of redox proteins on light-harvesting nanoparticles (including dye-sensitized TiO_2 nanoparticles);[17a-c] And, iii) site-selective, covalent labeling of redox proteins with Ru(bipyridine)$_3$-dyes[18a,b] (**Figure 1**a–c).

In this work, we developed a photosensitized-MtrC biohybrid by selective, covalent coupling to graphitic nitrogen-doped carbon dots (g-N-CDs) (Figure 1d). Carbon dots (CDs) have been shown as efficient and versatile redox-active photocatalytic materials for applications in light-driven transformations.[5g,19] The choice of CDs in this work was based on previous studies, which showed its feasibility to chemically modify their surface via several synthetic strategies.[5g,20] Additionally, their electrostatic interactions with molecular catalysts and enzymes have been explored for light-driven solar fuel production, demonstrating electron transfer from CDs to molecular catalysts and enzymes.[3c,21] Recently, we have shown that MtrC can be photoreduced by CDs in suspension.[16] However, direct, covalent coupling of CDs to

© 2023 The Authors. Advanced Functional Materials published by Wiley-VCH GmbH

16163028, 0, Downloaded from https://onlinelibrary.wiley.com/doi/10.1002/adfm.202302204 by University Of East Anglia, Wiley Online Library on [03/08/2023]. See the Terms and Conditions (https://onlinelibrary.wiley.com/terms-and-conditions) on Wiley Online Library for rules of use; OA articles are governed by the applicable Creative Commons License

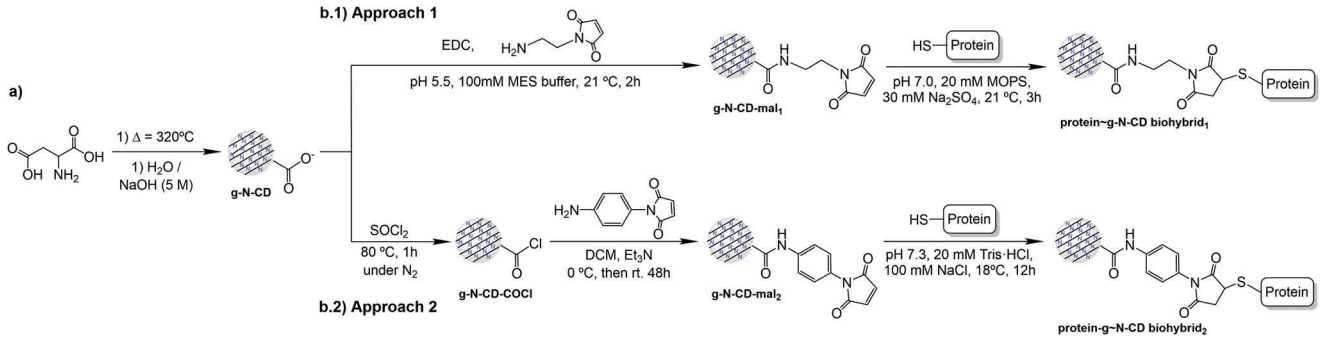

Scheme 1. Procedure for the synthesis of a) g-N-CD and their maleimide derivative functionalized g-N-CD using b.1) the carbodiimide or b.2) the acyl chloride activation strategies, respectively, and their respective attachment to a cysteine containing protein (named approach 1 and approach 2, respectively). EDC: 1-ethyl-3-carbodiimide hydrochloride.

biocatalysts for solar energy conversion has not yet been explored. Here, g-N-CDs are surface-functionalized with a maleimide-derivative by either carbodiimide chemistry or acyl chloride activation. To couple g-N-CDs to MtrC, a MtrC construct was used from which the native N-terminal lipid anchor was genetically removed.[22] This construct (named WT MtrC hereafter) contains 22 cysteine residues of which 20 cysteines are coupled to the 10 heme cofactors via thioether bonds in domain II and IV and 2 cysteines form a disulfide bond located on the surface of MtrC in Domain III (Figure 1e). A surface exposed tyrosine close to the terminus of the heme chain was mutated to a cysteine (Y657C MtrC), providing a single available thiol group for covalent linkage to maleimide modified g-N-CDs. Previous transient absorption spectroscopy with Y657C MtrC modified with a Ru(II)(2,2'-bipyridine)$_3$ dye on the cysteine confirmed ultrafast photoelectron transfer (< µs) from the Ru-dye to the heme chain.[18] WT and Y657C MtrC also carry C-terminal Strep II affinity tags to aid the biohybrids purification. Last, we show electron transfer from g-N-CDs to MtrC, suggesting it will be possible to drive photo-induced transmembrane electron transfer in *S. oneidensis* MR-1 for chemicals and fuels generation in the future.

2. Results and Discussion

2.1. Synthesis and Characterization of g-N-CDs and Maleimide Functionalized g-N-CDs

g-N-CDs were synthesized by pyrolysis of aspartic acid in air at 320 °C for 100 h (**Scheme 1**a), as previously reported.[21b] Dissolution in aqueous NaOH produced a dark brown solution, which was passed through a microfilter (0.22 µm) and freeze-dried to obtain a brown solid. Fluorescence emission spectroscopy, UV–vis spectroscopy, TEM characterization, ^{1}H NMR spectroscopy, and attenuated total reflectance Fourier transform infrared (ATR FT-IR) spectroscopy of the materials are consistent with previously reported data (Figures S1–S4, Supporting Information).[21b] The size of g-N-CDs is about 2.8 ± 0.2 nm (Figure S2, Supporting Information). Further modification of the g-N-CD with the maleimide derivative moiety was achieved following two different strategies: 1) traditional carbodiimide coupling chemistry to amine-modified maleimide (1-(2-aminoethyl)maleimide); and 2) thionyl chloride activation of the g-N-CD surface followed by amide bond formation with an amine-modified maleimide (4-(1-aminophenyl)maleimide) (Scheme 1b.1 and 1b.2, named approach 1 and 2, respectively). The carbodiimide chemistry used in approach 1 takes only a single step in aqueous phase at room temperature. However, it is harder to scale-up because the purification step for removing the excess EDC and maleimide leads to only part of the g-N-CD-mal fraction being available for the covalent coupling to the protein. The synthetic method in approach 2 takes two steps for maleimide modification, but the products can be produced on a larger scale. Moreover, despite both approaches use maleimide derivatives, it is worth mentioning that the linker is also different to compare the effect of having an aliphatic (g-N-CD-mal$_1$) or an aromatic (g-N-CD-mal$_2$) spacer in the electron transfer between g-N-CD and MtrC. Therefore, both approaches were explored to modify the g-N-CD with maleimide. Hereafter, we use the notation g-N-CD-mal$_1$ to indicate maleimide modification with approach 1 and g-N-CD-mal$_2$ for approach 2.

The g-N-CD-maleimide in approach 1 was synthesized through carbodiimide chemistry (Scheme 1b.1). Briefly, g-N-CD was reacted with 1-ethyl-3-carbodiimide hydrochloride (EDC) and 1-(2-aminoethyl)maleimide at 21 °C for 2 h in the dark. Excess EDC and 1-(2-aminoethyl)maleimide were removed by size exclusion chromatography (for details, see the Experimental Section). ATR FT-IR spectroscopy of g-N-CD-mal$_1$ shows the appearance of two new peaks at 1440 and 1409 cm^{-1}, which correspond to the N–H bending and C–N stretching modes of the amide bond and support that the maleimide derivative is covalently bound to the g-N-CD surface (Figure S5, Supporting Information). The peaks at 1367 and 1586 cm^{-1}, corresponding to the symmetric and antisymmetric C=O stretches of the carboxylic acid group of g-N-CDs, are still present,[21b] which indicates that not all the carboxylate groups were modified (Figure S5, Supporting Information). The C=O stretch of the amide bond is very likely hidden by the large C=O stretch peak of the carboxylate groups. The broad signal at 3500–2500 cm^{-1} is due to the N–H stretching of the amide bond, and O–H stretching of carboxylic acid and water. Additionally, ^{1}H NMR spectroscopy shows a new signal at 6.9 ppm in g-N-CD-mal$_1$ compared to g-N-CD, which is assigned to the –CH at the C=C bond of the maleimide derivative (Figure S6, Supporting Information), confirming the presence of the maleimide group in the g-N-CD-mal$_1$ product. No sharp peak feature of free maleimide was observed in the final g-N-CD-mal$_1$

© 2023 The Authors. Advanced Functional Materials published by Wiley-VCH GmbH

16163028, 0, Downloaded from https://onlinelibrary.wiley.com/doi/10.1002/adfm.202302204 by University Of East Anglia, Wiley Online Library on [03/08/2023]. See the Terms and Conditions (https://onlinelibrary.wiley.com/terms-and-conditions) on Wiley Online Library for rules of use; OA articles are governed by the applicable Creative Commons License

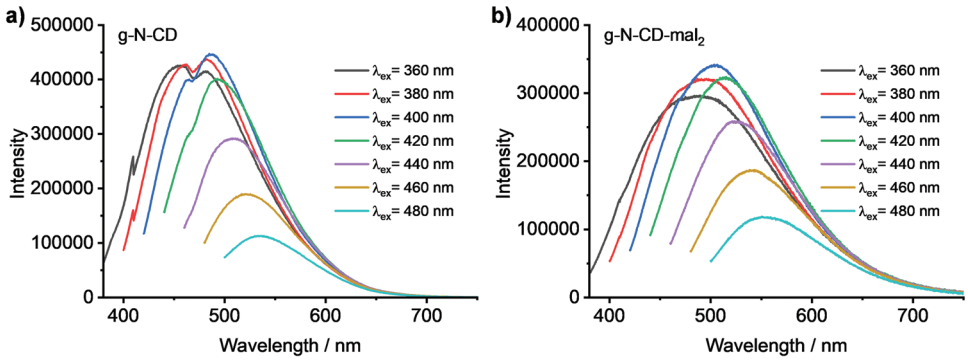

Figure 2. Fluorescence emission spectra at different excitation wavelengths (360, 380, 400, 420, 440, 460, and 480 nm) for the a) g-N-CD and b) g-N-CD-mal$_2$ in H_2O at pH 7.0, 21 °C. The results for samples prepared by approach 1 are shown in Figure S1 (Supporting Information).

^{1}H NMR spectrum, which shows that all excess maleimide starting material was removed by the size exclusion chromatography (Figure S6, Supporting Information).

The synthetic strategy of approach 2 was designed to activate the initial low reactive carboxylic acid surface groups of the starting g-N-CD by acyl chloride (Scheme 1b.2). Acyl chloride activation of the carboxylic acid groups of g-N-CD was carried out upon reaction with thionyl chloride at 80 °C under inert atmosphere, according to a previously reported procedure.[5g] This leads to acyl chloride modification of all the exposed carboxylic acid groups, as confirmed by ATR FT-IR spectroscopy from the shift of the carbonyl band from 1570 cm^{-1} in g-N-CD (g-N-CD-CO_2H) to 1704 cm^{-1} in g-N-CD-COCl (Figure S4, Supporting Information). Further reaction of g-N-CD-COCl with 4-(1-aminophenyl)maleimide (slow addition at 0 °C) in anhydrous dichloromethane (DCM) using triethylamine (Et_3N) as a base at room temperature for 2 days leads to the maleimide functionalized adducts (see Scheme 1b.2 and the Experimental Section for further details). The solvent was removed under reduced pressure, and the reaction crude was redispersed in dichloromethane, washed with water and neutralized to pH 7 by addition of aqueous HCl (1 M). The neutralized aqueous phase was freeze-dried and a brown solid was obtained. The reaction product g-N-CD-mal$_2$ was again analyzed by ATR FT-IR spectroscopy (Figure S4, Supporting Information). The peak at 1707 cm^{-1} disappeared, indicating g-N-CD-COCl was modified, and the amide C=O, N–H and C–N stretching frequencies at 1560, 1440, and 1400 cm^{-1} for g-N-CD-mal$_2$ confirms the amide bond formation between g-N-CD and the maleimide derivative. The ^{1}H-NMR spectrum of g-N-CD-mal shows a new set of aromatic signals absent in the initial g-N-CD that are most likely derived from the bound maleimide derivative, as suggested by the analyses of the latter ^{1}H-NMR spectrum (Figure S7, Supporting Information).

Both the g-N-CD and g-N-CD-maleimide particles in the two approaches show slightly different fluorescence and absorption properties for several reasons. First, the nature of the linker containing the maleimide derivative is different. Second, different extents of surface functionalization of the g-N-CD were achieved with the two different approaches. Finally, g-N-CD-mal$_1$ and a control sample (g-N-CD) were purified by a size exclusion column which removed some smaller size particles (for details, see the Experimental Section). With approach 2 there is more maleimide derivative functionalized on the surface as seen in the FTIR spectrum (Figures S4 and S5, Supporting Information). Although all fluorescence and absorption spectra of the g-N-CD and g-N-CD-mal samples are similar, we note that there is a more pronounced difference between the spectra of g-N-CD-mal and unmodified g-N-CD in approach 2 compared to approach 1 (**Figure 2**; and Figure S1, Supporting Information). Importantly, the g-N-CD-mal samples synthesized by both approaches retain their fluorescence and absorption properties.

2.2. Preparation and Characterization of Protein~g-N-CD Biohybrids

Protein~g-N-CD biohybrids were prepared following a general coupling strategy via the reaction of the maleimide in the g-N-CD-maleimide and the thiol of the surface-exposed cysteine residues (Scheme 1). First, proteins were treated with tris(2-carboxyethyl)phosphine hydrochloride (TCEP) for 20–30 min, following a similar reported procedure,[18c] to reduce any disulfide bonds between surface exposed cysteines (Figure 1e). After removing excess TCEP by ultrafiltration, g-N-CD-maleimide was added to react with the proteins. The reaction pH was kept below 7.5 to minimize side reactions between maleimide and other residues of the protein (lysines). Bovine Serum Albumin (BSA) was used as a model protein to demonstrate that this approach is universal for coupling g-N-CDs to proteins. The monomeric BSA has a molecular weight of 66.5 kDa. It contains 35 cysteine residues, which form 17 intramolecular disulfide bonds and one free cysteine residue to react with g-N-CD-maleimide (Figure S8, Supporting Information).[23] The same conjugation approach was subsequently applied to a MtrC mutant (Y657C MtrC) containing a freely exposed cysteine residue and the wild type MtrC (WT MtrC) as a control.

2.3. BSA~g-N-CD Biohybrids

Gel electrophoresis was used to confirm the formation of the BSA~g-N-CD biohybrids, as this method conveniently indicates protein modifications even with the presence of free, unreacted g-N-CD-maleimide (i.e., no purification of the biohybrid is required before analysis). Both sodium dodecyl sulfate–polyacrylamide gel

© 2023 The Authors. Advanced Functional Materials published by Wiley-VCH GmbH

16163028, 0, Downloaded from https://onlinelibrary.wiley.com/doi/10.1002/adfm.202302204 by University Of East Anglia, Wiley Online Library on [03/08/2023]. See the Terms and Conditions (https://onlinelibrary.wiley.com/terms-and-conditions) on Wiley Online Library for rules of use; OA articles are governed by the applicable Creative Commons License

16163028, 0, Downloaded from https://onlinelibrary.wiley.com/doi/10.1002/adfm.202302204 by University Of East Anglia, Wiley Online Library on [03/08/2023]. See the Terms and Conditions (https://onlinelibrary.wiley.com/terms-and-conditions) on Wiley Online Library for rules of use; OA articles are governed by the applicable Creative Commons License

electrophoresis (SDS-PAGE) and Native-PAGE were performed to provide qualitative information on the size and charge changes of BSA after conjugation to g-N-CD maleimide.

SDS-PAGE with proteins visualized by Coomassie Stain (**Figure 3**a) confirms that BSA does not covalently bind to g-N-CD unless the g-N-CDs are modified with maleimide (Figure 3a, lanes 1–3). g-N-CD is not stained by Coomassie Stain and hence not visible on the SDS-PAGE in Figure 3a (lane 5). The BSA∼g-N-CD biohybrid$_1$ (Figure 3a, lane 3) shows a broad band, migrating slower than BSA (Figure 3a, lane 1), in line with the larger size of the biohybrid compared to BSA. This relatively broad band of the BSA∼g-N-CD biohybrid$_1$ is expected, based on the heterogeneous size distribution of g-N-CDs. We note here that in SDS-PAGE, proteins migrate as unfolded polypeptides inside SDS micelles, where the SDS-polypeptide micelles are much larger than folded proteins.[24] This is in contrast to g-N-CD, which will neither unfold nor be bound to SDS micelles. Therefore, the change in migration due to the modification with g-N-CD is relatively small, in spite of the comparable size of g-N-CD (2.8 ± 0.2 nm) and BSA (about 7.1 nm when folded). Analysis of the other control samples confirmed the specific conjugation of BSA and g-N-CD-maleimide through formation of a maleimide-thiol bond. When reacting maleimide on the g-N-CD-mal$_1$ surface with 2-mercaptoethanol prior to additional of BSA, which should prevent coupling to the protein, the sample indeed migrates in a comparable manner to the original BSA sample (compare Figure 3a, lanes 1 and 4).

A complementary view of the contents of the samples described above was provided when the SDS-PAGE gels were visualized by fluorescence imaging with UV irradiation (Figure 3b).

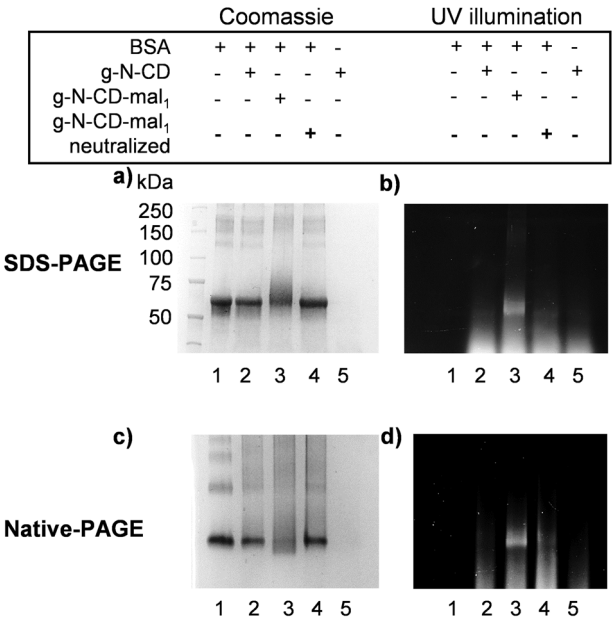

Figure 3. SDS-PAGE gel images of BSA samples visualized by a) Coomassie Stain and b) under UV illumination, Native-PAGE images of BSA samples visualized by c) Coomassie Stain and d) under UV illumination. Lanes: 1. BSA; 2. BSA/g-N-CD; 3. BSA∼g-N-CD biohybrid$_1$; 4. BSA/[g-N-CD-mal$_1$ neutralized by 2-mercaptoethanol]; 5. g-N-CD. Samples prepared by approach 1.

In this way the location of the g-N-CDs is directly revealed. The unreacted g-N-CDs in all samples migrate as a very broad band at the front (bottom in Figure 3b) of the gel due to its heterogeneity. However, the BSA∼g-N-CD biohybrids (Figure 3b lane 3) also show a faint fluorescent band at the location of BSA, which is not observed in the other samples. Hence this provides additional confirmation that BSA is covalently coupled to g-N-CDs through a thiol-maleimide linkage.

Comparable conclusions were reached from analysis of the samples by Native-PAGE. Proteins visualized by Coomassie Stain show that BSA∼g-N-CD biohybrid$_1$ migrates further than unmodified BSA (Figure 3c), which is attributed to the negative surface charge of g-N-CDs (Figure 3c, lane 3). Similar to SDS-PAGE, the BSA∼g-N-CD biohybrid$_1$ appears fluorescent from the g-N-CDs on Native-PAGE under UV illumination (Figure 3d, lane 3).

Size exclusion chromatography (SEC) was attempted to characterize and purify the BSA∼g-N-CD biohybrids (Figures S9 and S10, Supporting Information). However, separating BSA from g-N-CD by SEC proved very challenging due to the size heterogeneity of g-N-CD and elution profiles that do not conform to the expected protein/particle size. Altered elution profiles of assemblies between serum albumin and nanoparticles have been reported before,[25] and are likely due to varying weak interactions between the g-N-CD with the column resin. g-N-CDs elute along a broad elution volume, overlapping with BSA. Further, no significant difference was observed between nonreacted BSA control (BSA and g-N-CD mixture) and BSA∼g-N-CD biohybrids (BSA and g-N-CD-mal$_2$) (Figure S10, Supporting Information). UV–vis absorbance and fluorescence emission spectra confirm the g-N-CD is present in all the elution fractions (Figure S10, Supporting Information). Furthermore, the elution profile of the g-N-CD-maleimide and its BSA∼g-N-CD biohybrids was observed to depend on the exact nature of the resin and elution buffer, while g-N-CD-mal$_1$ elutes differently from g-N-CDs (Figure S9, Supporting Information). Nevertheless, SDS-PAGE shows the biohybrids are only formed when BSA reacts with g-N-CD-maleimide (Figure S9, Supporting Information). It was thus concluded that the SEC elution profile is consistent with biohybrid formation, but SEC cannot be used to purify BSA∼g-N-CD biohybrids from unreacted BSA and g-N-CD-maleimide. Finally, TEM analysis of the biohybrid samples also suggested the formation of the BSA∼g-N-CD biohybrids. In the TEM images the g-N-CDs (dark dots with graphitic fringes) can be seen within the protein scaffold (gray background shadow, Figure S10d, Supporting Information). Although unambiguous assignment of g-N-CD and BSA in the TEM images of the BSA∼g-N-CD biohybrid samples is challenging due to the low electron density of both BSA and g-N-CD, the TEM images are consistent with the possible formation of BSA∼g-N-CD biohybrids (Figure S10d, Supporting Information).

2.4. Y657C MtrC∼g-N-CD Biohybrids

2.4.1. Formation of Y657C MtrC∼g-N-CD Biohybrids

The methodology used for preparation and analysis of BSA∼g-N-CD biohybrids as described above was then applied to the labeling of the Y657C MtrC with g-N-CD-maleimide. As a control,

© 2023 The Authors. Advanced Functional Materials published by Wiley-VCH GmbH

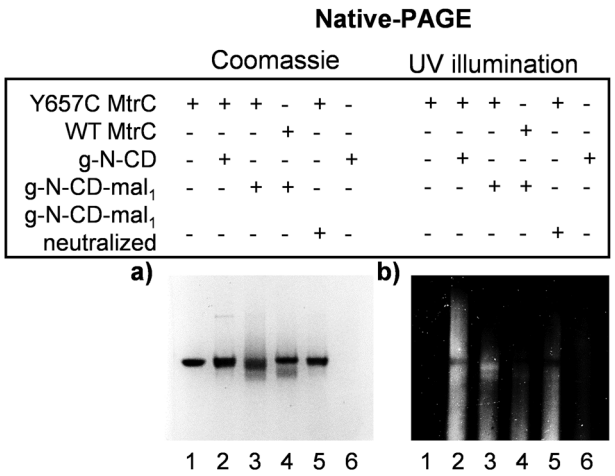

Figure 4. Native-PAGE images of MtrC samples visualized by a) Coomassie Stain and b) under UV illumination. Lanes: 1. Y657C MtrC, 2. Y657C MtrC/g-N-CD, 3. Y657C MtrC~g-N-CD biohybrid$_1$, 4. WT MtrC/g-N-CD-mal$_1$, 5. Y657C MtrC/[g-N-CD-mal$_1$ neutralizad by 2-mercaptoethanol], 6. g-N-CD. Samples prepared by approach 1.

parallel procedures were performed with WT MtrC, which lacks the surface reactive Cys at position 657. Similar to BSA samples, SDS-PAGE with proteins visualized by Coomassie Stain shows Y657C MtrC~g-N-CD biohybrid$_1$ appear as a slightly broadened band, migrating marginally slower than MtrC, although the difference in migration is much less clear than for BSA (Figure S11a, Supporting Information). Control samples in which g-N-CDs were not modified with maleimide or the maleimide was neutralized with 2-mercaptoethanol prior to the reaction appear identical to Y657C MtrC (Figure S11a, Supporting Information), as expected. Furthermore, reacting g-N-CD-mal$_1$ with WT MtrC, which does not have a surface exposed cysteine, indeed does not produce a change in migration on SDS-PAGE. The SDS-PAGE gel was also visualized under UV illumination to detect fluorescence from g-N-CD (Figure S11b, Supporting Information). However, in its denatured form MtrC has intrinsic fluorescence on an SDS-PAGE gel, as previously reported for cytochromes,[26] which makes it impossible to specifically detect fluorescence due to g-N-CD.

In Native-PAGE, modification with g-N-CD resulted in a diffuse, fluorescent band that migrated just below that of unmodified MtrC (**Figure 4**a,b, lane 3), which is attributed to the negatively charged g-N-CD. Unexpectedly, a much fainter band is also observed in the control sample with WT MtrC. While for Y657C MtrC~g-N-CD biohybrid, the sample as a whole migrates faster in Native-PAGE, for WT MtrC/g-N-CD-mal$_1$ an unexpected weak second band is visible (Figure 4a,b, lane 4), likely due to a partial side reaction or unspecific interaction between g-N-CD-mal$_1$ and MtrC.[5f] This is consistent with the fact that only the lower minor band in the WT MtrC/g-N-CD-mal$_1$ samples exhibits fluorescence.

The reaction mixture contains the Y657C MtrC~g-N-CD biohybrids, unreacted g-N-CD-mal, which is added in excess, and possibly unreacted Y657C MtrC. Because the unreacted g-N-CD-mal will interfere with the evaluation of the electron transfer between g-N-CD and MtrC in the biohybrids, further purification of the biohybrids from free g-N-CD-mal is necessary.

2.4.2. Size Exclusion Chromatography

As for BSA, SEC proved also very challenging for the purification of Y657C-g-N-CD biohybrids. Compared to the mixture of Y657C and g-N-CD, the Y657C MtrC~g-N-CD biohybrids elute later from a Superdex 200 Increase 10/300 GL column in borate buffer (**Figure 5**a). At first glance, this would suggest that the Y657C MtrC~g-N-CD biohybrid$_2$ is smaller than the unmodified Y657C MtrC. However, we speculate that the interactions between the g-N-CD and Superdex resin, as previously reported,[25] results in a retention of Y657C MtrC~g-N-CD biohybrid$_2$ and thus a delay in its elution. Indeed, when performed on Superdex 200 Increase 3.2/300 resin in MOPS buffer, Y657C MtrC~g-N-CD biohybrid$_1$ elute at a similar volume as unmodified Y657C MtrC (Figure S12, Supporting Information). UV–vis absorbance and fluorescence emission analysis are consistent with the Y657C MtrC~g-N-CD biohybrid$_2$ fractions containing both MtrC and g-N-CDs (Figure 5b,c). However, similar elution profiles were obtained with control experiments with either Y657C MtrC and g-N-CD (without maleimide modification) or WT MtrC (without cysteine mutation) and g-N-CD-mal$_2$ (Figure S13, Supporting Information). Importantly, SDS-PAGE and Native-PAGE confirm that covalent biohybrids are only formed with g-N-CD-maleimide (Figure S12b, Supporting Information). TEM images of Y657C MtrC~g-N-CD biohybrid$_2$ after SEC show the presence of CDs within the protein homogeneously in all the sample, suggesting the formation of the biohybrids (Figure 5d). In contrast, for the coeluted MtrC and g-N-CDs without prior covalent labeling upon incubation of MtrC with g-N-CD or g-N-CD-mal, the samples are heterogenous, showing parts of the sample grid containing only protein and other parts showing aggregates of g-N-CDs (Figure S13d, Supporting Information). The latter is in agreement with coeluted, but not covalently attached, protein and g-N-CDs. Taken together, this strongly suggests that noncovalent interactions between g-N-CD and MtrC as well as g-N-CDs and the SEC resin impair the purification of Y657C MtrC~g-N-CD biohybrids with size exclusion chromatography.

2.4.3. Strep-Tag Affinity Chromatography

As SEC chromatography appears challenging for purifying protein~g-N-CD biohybrids, affinity chromatography was explored. Since BSA does not contain any suitable affinity tags, affinity chromatography could not be used for its purification. However, MtrC carries a C-terminal Strep II-tag,[16b,18a] which thus offers the possibility to remove unreacted g-N-CD-maleimide from the biohybrids. UV–vis absorbance spectroscopy, fluorescence emission spectroscopy, and Native-PAGE were used to analyze the flow through (FT), washing (W), and elution (E) fractions of chromatography with Strep–Tactin resin as detailed in the Experimental Section.

The g-N-CD-mal$_1$ shows absorbance below 600 nm and a fluorescence emission when it is excited by UV light. The UV–vis spectrum and fluorescence emission spectrum of the flow

© 2023 The Authors. Advanced Functional Materials published by Wiley-VCH GmbH

16163028, 0, Downloaded from https://onlinelibrary.wiley.com/doi/10.1002/adfm.202302204 by University Of East Anglia, Wiley Online Library on [03/08/2023]. See the Terms and Conditions (https://onlinelibrary.wiley.com/terms-and-conditions) on Wiley Online Library for rules of use; OA articles are governed by the applicable Creative Commons License

16163028, 0, Downloaded from https://onlinelibrary.wiley.com/doi/10.1002/adfm.202302204 by University Of East Anglia, Wiley Online Library on [03/08/2023]. See the Terms and Conditions (https://onlinelibrary.wiley.com/terms-and-conditions) on Wiley Online Library for rules of use; OA articles are governed by the applicable Creative Commons License

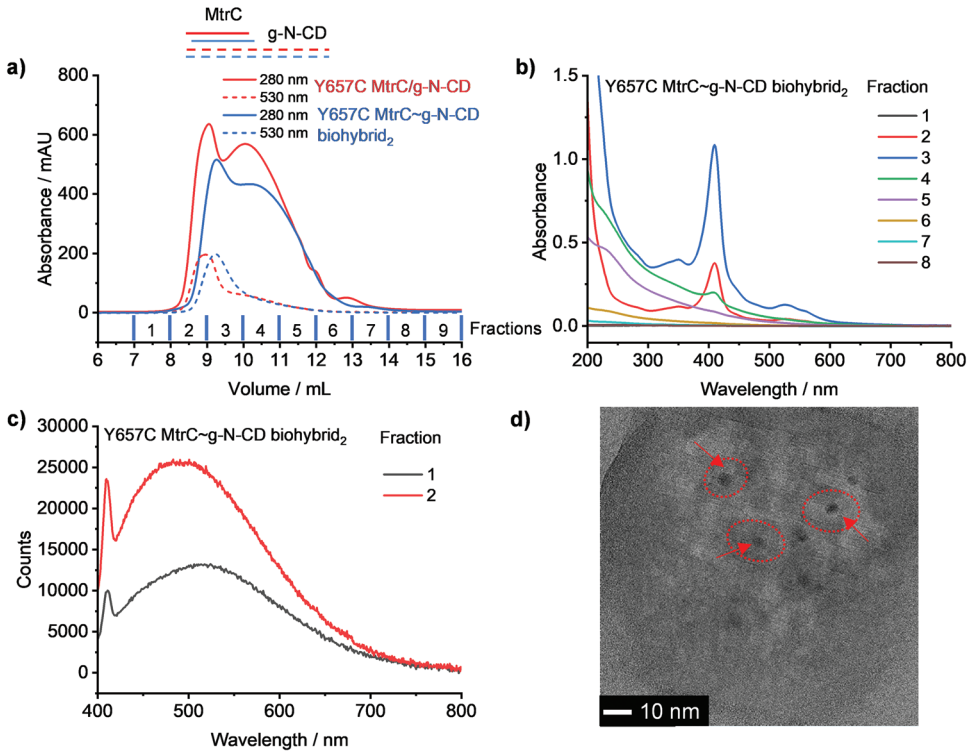

Figure 5. a) Elution profile on a Superdex 200 Increase 10/300 GL SEC column of mixtures of Y657C MtrC and g-N-CDs, and Y657C MtrC and g-N-CD-mal$_2$ after conjugation (pH 8.0, 20 mM borate buffer). b) UV-vis absorption and c) fluorescence (exited at 360 nm) spectra of SEC elution fractions as indicated in (a). d) TEM of Y657C MtrC~g-N-CD biohybrid$_2$ sample eluted at fraction 2. Arrows indicate 3 examples of electron density due to g-N-CD and circles indicate approximate electron density due to MtrC. Samples prepared by approach 2. The SEC results for samples prepared by approach 1 are shown in Figure S12 (Supporting Information).

through (FT) and wash (W) fractions (Figure S14, Supporting Information) confirm that the g-N-CD-mal$_1$ does not unspecifically bind to the Strep–Tactin resin so that these particles can be removed using standard washing step (**Figure 6**a, black trace). However, UV–vis spectroscopy indicates that in the presence of g-N-CDs, strep-tag MtrC binds less efficiently to the Strep–Tactin resin and even after a 16 h incubation, some protein appears in the washing steps. Note that there is more MtrC lost in the purification of the Y657C MtrC~g-N-CD biohybrid$_1$ sample compared to the WT MtrC/g-N-CD-mal$_1$ control sample (Figure S14, Supporting Information). We speculate that in the Y657C MtrC~g-N-CD biohybrid sample, the close proximity of g-N-CD to the C-terminal strep-tag interferes with the binding to the resin (residue 657 is close to the C-terminus of MtrC of 671 amino acids).

The elution (E) fractions were further characterized by UV–vis absorbance spectroscopy and fluorescence emission spectroscopy. Compared to Y657C MtrC alone, the absorbance at

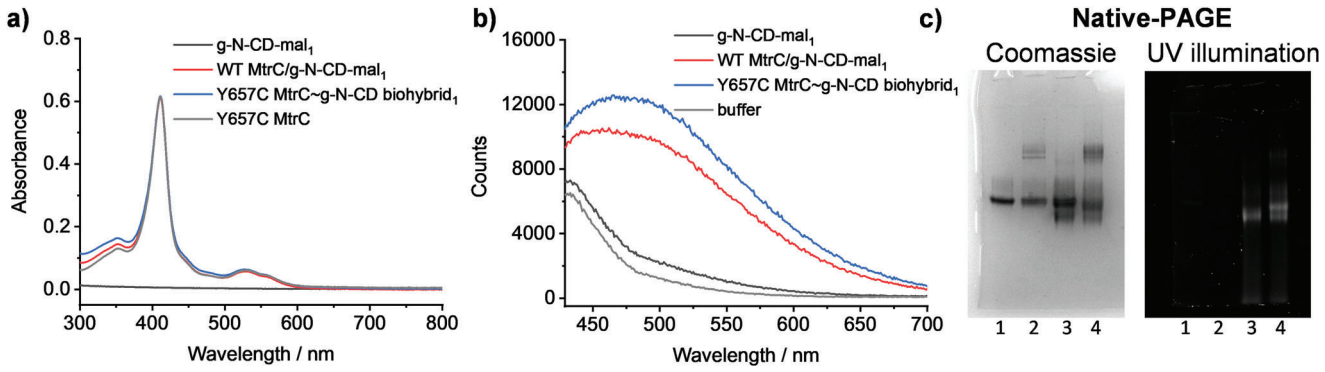

Figure 6. a) UV–vis absorption spectra and b) Fluorescence emission spectra of the strep tag column elution fractions. c) Native-PAGE images visualized by Coomassie Blue (left) and under UV illumination (right). Lanes: 1. WT MtrC, 2. Y657C MtrC, 3. Elution fraction of WT MtrC/g-N-CD-mal$_1$, 4. Elution fraction of Y657C MtrC~g-N-CD biohybrid$_1$. The slowest migrating bands in the Y657C MtrC samples (Figure 6c, lane 2 and 4) are MtrC dimers. Samples prepared by approach 1. pH 7.0, 20 mM MOPS, 30 mM Na_2SO_4, 21 °C.

© 2023 The Authors. Advanced Functional Materials published by Wiley-VCH GmbH

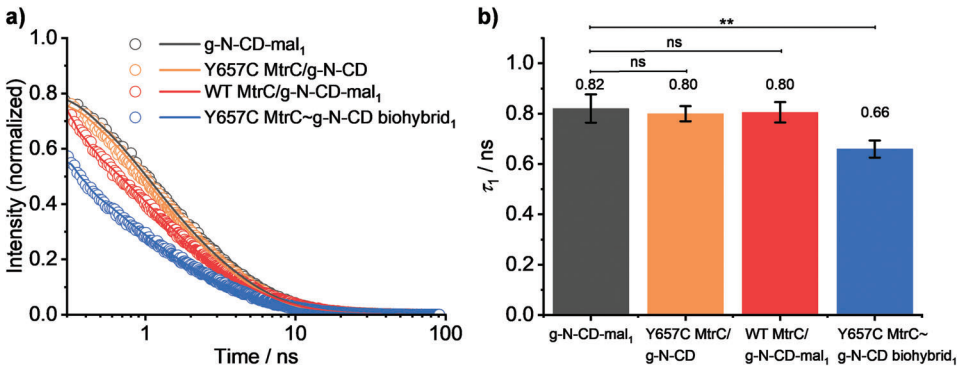

Figure 7. a) Fluorescence lifetime decay (circle) and fitting (solid line) curves, b) the shortest half-life time τ_1 of g-N-CD-mal$_1$, Y657C MtrC/g-N-CD (mixture without conjugation), WT MtrC/g-N-CD-mal$_1$ and Y657C MtrC~g-N-CD biohybrid$_1$. $^{**}p$-value = 0.008 (Data are the average of $n = 3$ datasets and error bars show standard deviation). Samples prepared by approach 1. The results of samples prepared by approach 2 are shown in Figure S15 (Supporting Information). pH 7.0, 20 mM MOPS, 30 mM Na_2SO_4, 21 °C anaerobic, excitation at 375 nm with emission measured at 475 nm. Fitting parameters are given in Table 1.

300 nm in the Y657C MtrC~g-N-CD biohybrid$_1$ elution sample is higher, consistent with the presence of g-N-CDs and thus biohybrid formation (Figure 6a). To a much lesser extent, UV–vis absorbance spectroscopy also indicates g-N-CDs in the WT MtrC/g-N-CD-mal$_1$ control sample, again consistent with the Native-PAGE result (Figure 4a,b), which indicates minor side reactions between g-N-CD-mal$_1$ and lysines or the (reduced) disulfide bond from WT MtrC and/or unspecific interaction between g-N-CD-mal$_1$ and MtrC. The g-N-CD concentration was estimated using the extinction coefficient of g-N-CD-mal$_1$ (1.25×10^5 M^{-1} cm^{-1}, details in the Experimental Section) and determined to be 106 ± 34% with respect to the concentration of the MtrC in the Y657C MtrC~g-N-CD biohybrid$_1$ sample. The g-N-CD concentration in the WT MtrC/g-N-CD-mal$_1$ control sample is 43 ± 24% respect to that of MtrC. The fluorescence emission spectrum (Figure 6b) further confirms the presence of g-N-CD in the samples and the fluorescence intensity of Y657C MtrC~g-N-CD biohybrid$_1$ is higher than that of WT MtrC/g-N-CD-mal$_1$, as expected.

The elution fractions were also characterized by Native-PAGE (Figure 6c). The Y657C MtrC~g-N-CD biohybrid$_1$ (Figure 6c, lane 4) appears as a broad fluorescent band below that of MtrC alone. In the WT MtrC/g-N-CD-mal$_1$ control sample (Figure 6c, lane 3) two bands are visible under Coomassie Stain, the main unmodified MtrC band and a lower minor band. Only the lower minor band in the WT MtrC/g-N-CD-mal$_1$ shows fluorescence under UV illumination and is again assigned to the side reaction coupling g-N-CD-mal$_1$ to WT MtrC.

Therefore, although SEC was unable to separate biohybrids from the Y657C MtrC and g-N-CD-maleimide reaction mixture, strep-tag affinity chromatography is a convenient method to separate unreacted g-N-CD-maleimide from Y657C MtrC~g-N-CD biohybrids.

2.5. Electron Transfer Study of MtrC~g-N-CD Biohybrid

The surface exposed cysteine of Y657C MtrC is located near the terminus of the heme chain (at a distance of 4.6 Å from sulfur of the cysteine to the heme edge[18a]). Thus, labeling of Y657C MtrC with g-N-CD is expected to bring heme and g-N-CD into sufficient proximity to allow for energy/electron transfer following excitation of the g-N-CD. This was explored by fluorescence lifetime measurements and photoreduction of MtrC during continuous irradiation in the presence of a sacrificial electron donor. The purified Y657C MtrC~g-N-CD biohybrids were used for the electron transfer study (details are in the Experimental Section).

2.5.1. Fluorescence Lifetime

Energy/electron transfer between g-N-CD and MtrC in the biohybrids was evaluated with fluorescence lifetime. The decays of lifetime curves and fitting curves are shown in **Figure 7**a; and Figure S15a (Supporting Information). The lifetime curves were fitted with a 3-exponential decay and considered the instrument response function (IRF). Two components of the exponential decay account for 77–92% of the total signal in all the samples and have relatively short lifetimes (τ_1 and τ_2) (**Table 1**; and Table S1, Supporting Information). The third component has a much longer lifetime (τ_3) and accounts for the remaining signal intensity (8–23%). The τ_1 in the Y657C MtrC~g-N-CD biohybrid samples becomes shorter than that of g-N-CD-maleimide (Figure 7b; and Figure S15b and Table 1; and Table S1, Supporting Information), indicating that in the Y657C MtrC~g-N-CD biohybrid, the lifetime of g-N-CD is shorter due to either electron transfer or energy transfer between g-N-CD and Y657C MtrC.[27] The lifetimes of g-N-CD in the mixture of Y657C MtrC and g-N-CD (without conjugation) and the WT MtrC/g-N-CD-maleimide control sample are not significantly affected, suggesting that only the specific coupling at the Cys mutant site, close to the heme edge, shortens the lifetime. If it is assumed that the shortening of fluorescence lifetime in the Y657C MtrC~g-N-CD biohybrid sample is solely due to electron transfer, and not for instance energy transfer, a rate constant for charge separation can be calculated of about 0.30×10^9 s^{-1} in the Y657C MtrC~g-N-CD biohybrid.

2.5.2. Cumulative Photoreduction

To obtain insight into the electron transfer properties within the biohybrids, the ability of g-N-CD to photoreduce Y657C

© 2023 The Authors. Advanced Functional Materials published by Wiley-VCH GmbH

16163028, 0, Downloaded from https://onlinelibrary.wiley.com/doi/10.1002/adfm.202302204 by University Of East Anglia, Wiley Online Library on [03/08/2023]. See the Terms and Conditions (https://onlinelibrary.wiley.com/terms-and-conditions) on Wiley Online Library for rules of use; OA articles are governed by the applicable Creative Commons License

Table 1. Half-life time of g-N-CD-mal$_1$, Y657C MtrC/g-N-CD (mixture without conjugation), WT/g-N-CD-mal$_1$, and Y657C MtrC~g-N-CD biohybrid$_1$. (Data are the average of $n = 3$ datasets and errors show standard deviation). Results for approach 2 are in Table S1 (Supporting Information).

	τ_1 [ns]	Percentage	τ_2 [ns]	Percentage	τ_3 [ns]	Percentage
g-N-CD-mal$_1$	0.82 ± 0.05	52.1 ± 0.7	2.96 ± 0.18	40.3 ± 0.9	9.19 ± 0.61	7.6 ± 0.8
Y657C MtrC/g-N-CD	0.80 ± 0.03	51.9 ± 0.9	2.77 ± 0.06	41.3 ± 0.8	8.49 ± 0.17	6.8 ± 0.2
WT MtrC/g-N-CD-mal$_1$	0.80 ± 0.04	51.3 ± 1.5	3.03 ± 0.25	40.5 ± 1.6	8.99 ± 0.48	8.1 ± 0.3
Y657C MtrC~g-N-CD biohybrid$_1$	0.66 ± 0.03	51.8 ± 1.0	2.84 ± 0.07	39.6 ± 0.6	8.87 ± 0.25	8.6 ± 0.5

MtrC was monitored by UV–vis spectroscopy during continuous irradiation under anaerobic conditions using ethylenediaminetetraacetic acid (EDTA) as a sacrificial electron donor, Figure 1d.[16a,b] MtrC photoreduction is conveniently determined by changes in absorbance of the Soret band. In the dark, the protein is fully oxidized with all hemes in the Fe(III) state as indicated by the maximum absorbance at 410 nm of the Soret band (Figures S16 and S17, black trace, Supporting Information). Fully reduced MtrC shows an intense Soret band with maximum absorbance at 420 nm (Figure S17, red traces, Supporting Information). The WT MtrC with g-N-CD-mal$_2$ in situ mixture (without preparation procedures for conjugation) shows a shift of the Soret band from 410 to 420 nm with irradiation (Figure S16, Supporting Information), indicating that reduction takes place when there is no covalent binding, consistent with previous reports.[12c,16a] This also shows that the g-N-CD-maleimide can still transfer electron to MtrC after maleimide modification. The time course of the photoreduction (**Figure 8**) shows that Y657C MtrC~g-N-CD biohybrids are almost fully reduced after 60 min irradiation. In the first 60 min, the photoreduction efficiency is higher in the Y657C MtrC~g-N-CD biohybrid sample than that of the control sample WT MtrC/g-N-CD-mal$_1$ (prepared with the conjugation procedure). There is no significant reduction of MtrC observed without EDTA, light or g-N-CD for the Y657C MtrC samples (Figure 8).

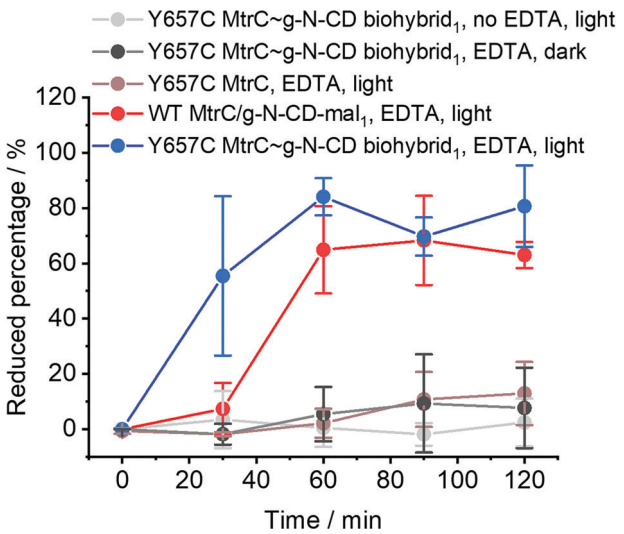

Figure 8. Time course changes under different conditions for Y657C MtrC, WT MtrC/g-N-CD-mal$_1$, and Y657C MtrC~g-N-CD biohybrid$_1$, percentage of reduced MtrC defined by optical absorbance spectroscopy (Data are the average of $n = 3$ datasets and error show standard deviation for the WT MtrC/g-N-CD-mal$_1$ and Y657C MtrC~g-N-CD biohybrid$_1$ with illumination in the presence of EDTA). 500 mM EDTA in anaerobic pH 8.5, 20 mM Tris, 100 mM NaCl. Samples prepared by approach 1. The results of samples prepared by approach 2 are shown in Figure S16 (Supporting Information).

Thus, photoreduction of MtrC by the covalently coupled g-N-CD was achieved in the Y657C MtrC~g-N-CD biohybrid. The cumulative photoreduction of the MtrC occurs on the timescale of tens of minutes even though the fluorescence lifetime of the Y657C MtrC~g-N-CD biohybrid suggests that the electron transfer from g-N-CD to MtrC, i.e., charge separation, is much faster. A similar behavior was previously observed for Y657C MtrC labeled with a Ru(II)(2,2'-bipyridine)$_3$ dye on the 657 cysteine position (RuMe-MtrC). Cumulative photoreduction of RuMe-MtrC in the presence of a sacrificial electron donor took about 1 h,[16b] despite a fast charge separation rate ($k_{CS} \approx 100 \times 10^6$ s^{-1}) determined by time-resolved photoluminescence spectroscopy and transient absorbance spectroscopy.[18a] For RuMe-MtrC these observations were reconciled by noting that cumulative photoreduction requires that the hole of the photosensitiser in the charge separated state is filled by oxidation of the sacrificial electron donor before charge recombination ($k_{CR} = 301 \times 10^6$ s^{-1})[18a] returns the system to its ground state (Figure S18, Supporting Information). It is thus likely that for the MtrC~g-N-CD biohybrid a fast charge recombination outcompetes the EDTA oxidation, thus explaining the cumulative photoreduction rates reported here.

3. Conclusions

We have developed a biohybrid by covalently modifying cysteine containing proteins with maleimide-modified g-N-CDs. The surface modification of g-N-CD with maleimide derivatives was achieved by two synthetic approaches, either carbodiimide chemistry or acyl chloride activation. The successful formation of the MtrC~g-N-CD biohybrids was supported by SDS-PAGE and Native-PAGE, with some unspecific reaction between MtrC and g-N-CD-maleimide as shown with WT MtrC. No significant difference was observed between MtrC~g-N-CD biohybrids prepared with the two synthetic approaches, even though acyl chloride activation could potentially lead to a higher coverage of maleimide. We also do not observe a significant difference in life-time fluorescence, suggesting the different linkers (ethyl vs phenyl) do not affect the particles nor their interaction with MtrC. Both approaches are straightforward and can be applied to assess the labeling of other proteins and enzymes with CDs.

Although the reaction between maleimide-modified g-N-CDs and cysteines is simple and efficient, purification of the

© 2023 The Authors. Advanced Functional Materials published by Wiley-VCH GmbH

16163028, 0, Downloaded from https://onlinelibrary.wiley.com/doi/10.1002/adfm.202302204 by University Of East Anglia, Wiley Online Library on [03/08/2023]. See the Terms and Conditions (https://onlinelibrary.wiley.com/terms-and-conditions) on Wiley Online Library for rules of use; OA articles are governed by the applicable Creative Commons License

biohybrids requires special attention. Size exclusion chromatography appears challenging due to electrostatic interactions between g-N-CDs and proteins and unspecific interactions between g-N-CDs and the chromatography resin. Affinity chromatography such as strep-tag affinity chromatography provides good results and the biohybrids were purified with almost all free g-N-CDs removed. UV–vis spectroscopy, fluorescence emission spectroscopy, and Native-PAGE were used to confirm the formation and purification of Y657C MtrC∼g-N-CD biohybrids. The fluorescence lifetime is shorter for the biohybrids due to either electron transfer or energy transfer after conjugation. Moreover, photoreduction studies monitored by UV–vis spectroscopy show the reduction of the MtrC heme groups from Fe(III) to Fe(II) under light irradiation in the presence of EDTA as sacrificial electron donor. This observation supports electron transfer from g-N-CD to the MtrC within the biohybrid, demonstrating that covalent biohybrids between carbon dots and redox proteins can support photoinduced electron transfer. Using g-N-CDs as the light-absorber will lead to a more sustainable system due to its tunable structure, low cost, and biocompatibility.

MtrC∼g-N-CD biohybrids could find a potential application in various reaction systems, such as liposomal microreactors for photocatalysis. For instance, we have recently shown an example of microreactors with encapsulated N_2O reductase for the photochemical reduction of N_2O.[16] Moreover, MtrC∼g-N-CD biohybrids can potentially be applied in whole cells of *S. oneidensis* MR-1. Previous (noncovalent) biohybrids of *S. oneidensis* MR-1 have shown biophotocatalysis for, for instance, hydrogen production.[12d] Another example shows *S. oneidensis* MR-1 respiring on hydrocarbons that acted as electron donor to supply electrons for photocatalytic hydrogen evolution outside the cells.[28] In the future, we envision that MtrC∼g-N-CD biohybrids can be reassembled into whole *S. oneidensis* MR-1 to drive organic synthesis inside the cell with fuel production (e.g., CO_2 reduction) outside the bacterium, where the covalently linked MtrC∼g-N-CD biohybrid provides a well-defined transmembrane electron transfer pathway to efficiently drive the whole-cell biocatalyst.

4. Experimental Section

Materials and Reagents: Reagents and solvents were purchased from commercial sources and used as received unless otherwise stated: deuterium oxide (Sigma-Aldrich, 99.9 atom % D), deuterated methanol (Sigma-Aldrich, 99.9 atom % D), ethanol (VWR Chemicals), 2-propanol (Honeywell), diethylether (Sigma-Aldrich, HPLC grade), dichloromethane (Sigma-Aldrich, HPLC grade), acetonitrile (Fischer Scientific, HPLC grade), ethyl acetate (Sigma-Aldrich, HPLC grade), sulfuric acid (Fisher Chemical, >95%), hydrochloric acid (Sigma-Aldrich, >95%), thionyl chloride (Sigma-Aldrich, reagent grade, 97%), tris(hydroxymethyl)aminomethane (Tris, Sigma-Aldrich), tris(2-carboxyethyl)phosphine (TCEP, Sigma-Aldrich), 1-(2-aminoethyl)maleimide hydrochloride (Sigma-Aldrich), 4-(1-aminophenyl)maleimide (TCI Chemicals, >93.0%), (1-ethyl-3-(3-dimethylaminopropyl)carbodiimide hydrochloride) (EDC, Thermo Fisher), Albumin Bovine Fraction V (BSA, Melford), 2-mercaptoethanol (Sigma-Aldrich), 4-morpholineethanesulfonic acid (MES, Sigma-Aldrich), ethylenediaminetetraacetic acid (EDTA, Sigma-Aldrich). Sodium formate (Sigma-Aldrich, ≥99.0%) was dried before use. Millipore water (18.2 MΩ cm at 25 °C) was used throughout this work. Solvents used for synthesis such as tetrahydrofuran (THF), triethylamine (Et_3N), dimethylformamide (DMF), and dichloromethane (DCM) were distilled on sodium (THF) or calcium hydride (Et_3N, DMF, and DCM) before use.

Characterization: ^{1}H Nuclear magnetic resonance (NMR) spectra were recorded on the following Bruker spectrometers: a 400 MHz Avance III (BBO Probe), a 500 MHz AV III (BBO Smart Probe), an Avance 500 TCI Cryoprobe (TCI and ATM cryoprobe) or a Bruker AV-III-HD-850 spectrometer under standard conditions (298 K) unless otherwise indicated. All ^{1}H chemical shifts are reported in ppm and have been internally calibrated to H_2O or the residual protons of the deuterated solvent. The ^{13}C chemical shifts have been internally calibrated to the carbon atoms of the deuterated solvent. UV–visible spectroscopy was carried out on a Agilent Gary 60 Spectrophotometer or a Portable Ocean Optics UV–vis using quartz cuvettes with 1 cm path length. Infrared spectra were obtained with a Thermo Scientific Nicolet iS50 FT-IR spectrometer or PerkinElmer Spectrum Two FT-IR Spectrometer. Fluorescence Emission spectra were recorded using a spectrofluorometer (FS5 Spectrofluorometer, Edinburgh Instrument or a PicoQuant FluoTime 300) at the indicated excitation wavelengths in a cuvette with a 1 cm path length. Fluorescence lifetime measurements were taken with excitation wavelength at 375 or 360 nm and emission wavelength at 475 nm. Transmission electron microscopy (TEM) images were collected using a Thermo Scientific (FEI) Talos F200X G2 TEM operating at 200 kV. TEM images were acquired using a Ceta 16 M CMOS camera. Samples were prepared by applying 5 µL of the suspended sample in an aqueous solution onto continuous carbon 300 mesh Cu grids that were negative glow discharged using a Quorum Technologies GloQube.

MtrC Protein Expression and Purification: WT and Y657C MtrC, lacking the lipid attachment site of wild-type MtrC and carrying a C-terminal Strep II affinity tag, were obtained following a previously reported procedure[16b,18a,22] and directly used. Briefly, proteins were produced by *Shewanella oneidensis* MR-1 after expression from the corresponding gene inserted into a pBAD202/D-TOPO vector. Purification from the spent media was by high-capacity Strep-Tactin XT Superflow column (5 mL, IBA Solutions for Life Sciences).

Synthesis of g-N-CD and g-N-CD-Maleimide: N-doped graphitic carbon dots (g-N-CDs) were synthesized by pyrolysis of L-aspartic acid at 320 °C for 100 h according to previously published procedures.[29]

The g-N-CD-mal$_1$ (approach 1) was synthesized by carbodiimide chemistry. g-N-CD (10 mg mL^{-1}) was mixed with 1-(2-aminoethyl)maleimide hydrochloride (10 mM) in pH 5.5, 100 mM MES buffer. After addition of EDC to an end concentration of 20 mM, the mixture was incubated for 2 h at 21 °C in the dark. Excess 1-(2-aminoethyl)maleimide hydrochloride and EDC was removed by NAP-5 desalting column (Cytiva) (equilibration and elution buffer is pH 7.0, 20 mM MOPS, 30 mM Na_2SO_4). The reaction mixture sample (0.1 mL) was loaded in each column and buffer (0.4 mL) was added. 0.5 mL of the eluent was collected which contains g-N-CD-mal$_1$. For ATR FT-IR and ^{1}H NMR spectroscopy, the g-N-CD and g-N-CD-mal$_1$ were eluted with Milli-Q H_2O instead of buffer (NAP-5 desalting column was equilibrated with Milli-Q H_2O), followed by freeze drying. The extinction coefficient of g-N-CD-mal$_1$ was calculated based on the slope of absorbance at 300 nm using a serial dilution of a g-N-CD-mal$_1$ solution with known concentration.

The g-N-CD-mal$_2$ (approach 2) was synthesized by thionyl chloride activation of g-N-CD surface followed by amide bond formation with a maleimide derivative. g-N-CD-COCl was prepared in a similar manner as previously reported for amorphous carbon dots[5g] by refluxing g-N-CD (250.0 mg) in neat thionyl chloride (12 mL) at 80 °C under an N_2 atmosphere for 2 h. Thionyl chloride was removed under reduced pressure, and the resulting g-N-CD-COCl was dissolved in dry THF (5 mL) and filtered. The solvent was evaporated under high vacuum at 40 °C to yield acyl chloride capped g-N-CDs (204.5 mg, 82% yield). Then a dichloromethane (anhydrous) solution (10 mL) containing CD-COCl (204.5 mg) was added dropwise at 0 °C to a solution of 4-(1-aminophenyl)maleimide (1.0 mg, 9.1 mmol) and Et_3N (1 mL, 36 eq.) in dichloromethane (8 mL). The yellowish solution was left stirring 2 days at room temperature. The solvent was removed under reduced pressure, redispersed in dichloromethane, washed with aqueous HCl (1 M) and then neutralized to pH 7. Elemental

© 2023 The Authors. Advanced Functional Materials published by Wiley-VCH GmbH

16163028, 0, Downloaded from https://onlinelibrary.wiley.com/doi/10.1002/adfm.202302204 by University Of East Anglia, Wiley Online Library on [03/08/2023]. See the Terms and Conditions (https://onlinelibrary.wiley.com/terms-and-conditions) on Wiley Online Library for rules of use; OA articles are governed by the applicable Creative Commons License

analysis found: C, 34.79%; H, 5.51%; N, 7.41%, whereas for the initial g-N-CD-CO_2H was C, 39.46%; H, 2.36%; N, 13.43%.

Synthesis of Protein~g-N-CD Biohybrids: The proteins (BSA or MtrC, the concentration of BSA was calculated using a molecular weight of 66.5 kDa and the concentration of MtrC was calculated using an extinction coefficient of 1326 mM^{-1} cm^{-1} at 410 nm) were first reduced by adding 10–15 fold TCEP and incubated for 20–30 min at 21 °C in either pH 7.0, 20 mM MOPS, 30 mM Na_2SO_4 or pH 7.0, 20 mM Tris, 100 mM NaCl. TCEP and its oxidation product were separated from the reduced protein by centrifugal filtration in spin concentrators (30 kDa cut-off). Labeling proteins with g-N-CD-mal$_1$ was performed in pH 7.0, 20 mM MOPS, 30 mM Na_2SO_4 buffer. The reduced protein (10 µM) was added into a solution containing g-N-CD-mal$_1$ at volume ratio of 1:1 (molar ratio is around 1:10) and the samples were incubated at 21 °C for 3 h under dark. Labeling of the proteins with g-N-CD-mal$_2$ was performed in pH 7.3, 20 mM Tris-HCl buffer, 100 mM NaCl. The reduced proteins (≈40µM) were added to about 10-fold molar excess of g-N-CD-mal$_2$ and then incubated in a bacterial shaker overnight at 50 rpm and 18 °C. The bioconjugate reaction crude was buffer exchanged by centrifugal filtration in spin concentrators (30 kDa cut-off) to pH 8.0, 20 mM borate buffer for further purification by SEC and frozen at −80 °C until used.

Purification of Protein~g-N-CD Biohybrids: Size exclusion chromatography was performed on an ÄKTA pure with either a Superdex 200 Increase 10/300 GL prepacked column (Cytiva) or Superdex 200 increase 3.2/300 prepacked column (Cytiva). The columns were equilibrated with either pH 8.0, 20 mM borate buffer (to partially suppress CD-matrix interaction facilitating the purification in the case of protein~g-N-CD biohybrid$_2$) or with pH 7.4, 20 mM MOPS, 30 mM Na_2SO_4 (in the case of protein~g-N-CD biohybrid$_1$) (2 column volumes). The reaction mixtures (up to 0.5 mL for Superdex 200 Increase 10/300 GL or 40 µL for the Superdex 200 Increase 3.2/300) were injected to the column via a loop. The column was eluted at the manufacturers recommended flow rate. The purified samples were used for electron transfer study (fluorescence lifetime and photoreduction).

Affinity chromatography of reaction mixtures was performed with Strep-Tactin XT 4Flow resin (IBA Lifesciences). 500 µL Y657C MtrC~g-N-CD biohybrid$_1$ or WT MtrC/g-N-CD-mal$_1$ sample (5 µM MtrC) was diluted into 1.5 mL (pH 7.0, 20 mM MOPS, 30 mM Na_2SO_4) and then mixed with 0.5 mL bed volume resin. The mixture was rotated for 16 h at 4 °C and poured into an empty column the next day. The flow through, washing (10 column volumes) and elution fraction (1.5 column volumes) were collected. The washing buffer is pH 8.0, 100 mM Tris-Cl, 150 mM NaCl, 1 mM EDTA. The elution buffer is 50 mM biotin in washing buffer. The elution fraction was buffer exchanged into pH 7.0, 20 mM MOPS, 30 mM Na_2SO_4 buffer by centrifugal filtration in spin concentrators (30 kDa cut-off). The purified samples were used for electron transfer study (fluorescence lifetime and photoreduction).

Photoreduction of Biohybrids: The photoreduction experiments were performed in a MBraun glovebox (O_2 < 1 ppm) at 20 °C with 500 mM EDTA (pH 8.5, 20 mM Tris-HCl, 100 mM NaCl) as the sacrificial electron donor. The samples were irradiated by a cold light source holding a 150 W (15 V) halogen lamp (OSRAM) with a fiber optic arm (Krüss KL5125) or with a LED (8.75 W, λ = 385 nm). The samples were in a quartz cuvette and placed 2 cm from the light source when irradiated. The light intensity at the sample under these conditions was ≈450 ± 40 mW cm^{-2} at 400 nm for the halogen lamp irradiation and 5.1 ± 0.1 W cm^{-2} at 385 nm. After the desired irradiation time, the absorbance spectrum was taken. After irradiation for 2 h, additional dithionite was added to fully reduce MtrC. The absorbance at 420 nm of the fully reduced MtrC was used as 100% reduction to determine the reduced percentage at the different illumination times.

Supporting Information

Supporting Information is available from the Wiley Online Library or from the author.

Acknowledgements

The authors thank Dr. Simone Payne for assistance with purification of MtrC proteins and Dr. Penny Hamlyn from Cytiva for valuable discussions about GF-SEC. The authors acknowledge the UK Biotechnology and Biological Sciences Research Council for funding (Nos. BB/S002499/1, BB/S00159X/1, and BB/S000704/1). The European Commission is acknowledged for a Marie Sklodowska-Curie Individual Fellowship to CC (No. 890745-SmArtC) and the EPSRC Multi-User Equipment Call (No. EP/P030467/1) for funding.

Conflict of Interest

The authors declare no conflict of interest.

Author Contributions

H.Z. and C.C. contributed equally to this work. The manuscript was written through contributions of all authors. All authors have given approval to the final version of the manuscript.

Data Availability Statement

The data that support the findings of this study are openly available at https://doi.org/10.17863/CAM.99587.

Keywords

biohybrids, covalent protein labeling, nanoparticles, semiartificial photosynthesis, solar fuels

Received: February 24, 2023
Revised: May 12, 2023
Published online:

[1] N. Kornienko, J. Z. Zhang, K. K. Sakimoto, P. Yang, E. Reisner, *Nat. Nanotechnol.* **2018**, *13*, 890.
[2] a) K. K. Sakimoto, A. B. Wong, P. Yang, *Science* **2016**, *351*, 74; b) S. Cestellos-Blanco, H. Zhang, J. M. Kim, Y.-x. Shen, P. Yang, *Nat. Catal.* **2020**, *3*, 245; c) S. H. Lee, D. S. Choi, S. K. Kuk, C. B. Park, *Angew. Chem., Int. Ed.* **2018**, *57*, 7958.
[3] a) J. Z. Zhang, K. P. Sokol, N. Paul, E. Romero, R. van Grondelle, E. Reisner, *Nat. Chem. Biol.* **2016**, *12*, 1046; b) X. Fang, S. Kalathil, E. Reisner, *Chem. Soc. Rev.* **2020**, *49*, 4926; c) V. M. Badiani, C. Casadevall, M. Miller, S. J. Cobb, R. R. Manuel, I. A. C. Pereira, E. Reisner, *J. Am. Chem. Soc.* **2022**, *144*, 14207.
[4] J. K. Utterback, J. L. Ruzicka, H. R. Keller, L. M. Pellows, G. Dukovic, *Annu. Rev. Phys. Chem.* **2020**, *71*, 335.
[5] a) K. A. Brown, S. Dayal, X. Ai, G. Rumbles, P. W. King, *J. Am. Chem. Soc.* **2010**, *132*, 9672; b) B. L. Greene, C. A. Joseph, M. J. Maroney, R. B. Dyer, *J. Am. Chem. Soc.* **2012**, *134*, 11108; c) M. B. Wilker, K. E. Shinopoulos, K. A. Brown, D. W. Mulder, P. W. King, G. Dukovic, *J. Am. Chem. Soc.* **2014**, *136*, 4316; d) K. A. Brown, M. B. Wilker, M. Boehm, G. Dukovic, P. W. King, *J. Am. Chem. Soc.* **2012**, *134*, 5627; e) J. K. Utterback, M. B. Wilker, K. A. Brown, P. W. King, J. D. Eaves, G. Dukovic, *Phys. Chem. Chem. Phys.* **2015**, *17*, 5538; f) K. Holá, M. V. Pavliuk, B. Németh, P. Huang, L. Zdražil, H. Land, G. Berggren, H. Tian, *ACS Catal.* **2020**, *10*, 9943; g) G. A. M. Hutton, B. Reuillard, B. C. M. Martindale, C. A. Caputo, C. W. J. Lockwood, J. N. Butt, E. Reisner, *J. Am. Chem. Soc.* **2016**, *138*, 16722; h) C. A. Caputo, L. Wang, R. Beranek, E. Reisner, *Chem. Sci.* **2015**, *6*, 5690.

© 2023 The Authors. Advanced Functional Materials published by Wiley-VCH GmbH

16163028, 0, Downloaded from https://onlinelibrary.wiley.com/doi/10.1002/adfm.202302204 by University Of East Anglia, Wiley Online Library on [03/08/2023]. See the Terms and Conditions (https://onlinelibrary.wiley.com/terms-and-conditions) on Wiley Online Library for rules of use; OA articles are governed by the applicable Creative Commons License

[6] a) Y. S. Chaudhary, T. W. Woolerton, C. S. Allen, J. H. Warner, E. Pierce, S. W. Ragsdale, F. A. Armstrong, *Chem. Commun.* **2012**, *48*, 58; b) L. Zhang, M. Can, S. W. Ragsdale, F. A. Armstrong, *ACS Catal.* **2018**, *8*, 2789; c) M. Miller, W. E. Robinson, A. R. Oliveira, N. Heidary, N. Kornienko, J. Warnan, I. A. C. Pereira, E. Reisner, *Angew. Chem., Int. Ed.* **2019**, *58*, 4601.

[7] H. Hamby, B. Li, K. E. Shinopoulos, H. R. Keller, S. J. Elliott, G. Dukovic, *Proc. Natl. Acad. Sci. USA* **2020**, *117*, 135.

[8] K. A. Brown, D. F. Harris, M. B. Wilker, A. Rasmussen, N. Khadka, H. Hamby, S. Keable, G. Dukovic, J. W. Peters, L. C. Seefeldt, P. W. King, *Science* **2016**, *352*, 448.

[9] Y. Pellegrin, F. Odobel, *C. R. Chim.* **2017**, *20*, 283.

[10] A. Pannwitz, D. M. Klein, S. Rodríguez-Jiménez, C. Casadevall, H. Song, E. Reisner, L. Hammarström, S. Bonnet, *Chem. Soc. Rev.* **2021**, *50*, 4833.

[11] H. Zhang, H. Liu, Z. Tian, D. Lu, Y. Yu, S. Cestellos-Blanco, K. K. Sakimoto, P. Yang, *Nat. Nanotechnol.* **2018**, *13*, 900.

[12] a) A. M. Wroblewska-Wolna, A. J. Harvie, S. F. Rowe, K. Critchley, J. N. Butt, L. J. C. Jeuken, *Nanotechnology* **2020**, *31*, 134005; b) H. Shen, Y.-Z. Wang, G. Liu, L. Li, R. Xia, B. Luo, J. Wang, D. Suo, W. Shi, Y.-C. Yong, *ACS Catal.* **2020**, *10*, 13290; c) S. F. Rowe, G. L.e Gall, E. V. Ainsworth, J. A. Davies, C. W. J. Lockwood, L. Shi, A. Elliston, I. N. Roberts, K. W. Waldron, D. J. Richardson, T. A. Clarke, L. J. C. Jeuken, E. Reisner, J. N. Butt, *ACS Catal.* **2017**, *7*, 7558; d) H.-X. Han, L.-J. Tian, D.-F. Liu, H.-Q. Yu, G.-P. Sheng, Y. Xiong, *J. Am. Chem. Soc.* **2022**, *144*, 6434; e) B. Luo, Y.-Z. Wang, D. Li, H. Shen, L.-X. Xu, Z. Fang, Z. Xia, J. Ren, W. Shi, Y.-C. Yong, *Adv. Energy Mater.* **2021**, *11*, 2100256.

[13] X. Guan, S. Erşan, X. Hu, T. L. Atallah, Y. Xie, S. Lu, B. Cao, J. Sun, K. Wu, Y. Huang, X. Duan, J. R. Caram, Y. Yu, J. O. Park, C. Liu, *Nat. Catal.* **2022**, *5*, 1019.

[14] G. F. White, Z. Shi, L. Shi, Z. Wang, A. C. Dohnalkova, M. J. Marshall, J. K. Fredrickson, J. M. Zachara, J. N. Butt, D. J. Richardson, *Proc. Natl. Acad. Sci. USA* **2013**, *110*, 6346.

[15] M. J. Edwards, G. F. White, J. N. Butt, D. J. Richardson, T. A. Clarke, *Cell* **2020**, *181*, 665.

[16] a) A. Stikane, E. T. Hwang, E. V. Ainsworth, S. E. H. Piper, K. Critchley, J. N. Butt, E. Reisner, L. J. C. Jeuken, *Faraday Discuss.* **2019**, *215*, 26; b) S. E. H. Piper, M. J. Edwards, J. H. van Wonderen, C. Casadevall, A. Martel, L. J. C. Jeuken, E. Reisner, T. A. Clarke, J. N. Butt, *Front. Microbiol.* **2021**, *12*, 714508; c) S. E. H. Piper, C. Casadevall, E. Reisner, T. A. Clarke, L. J. C. Jeuken, A. J. Gates, J. N. Butt, *Angew. Chem., Int. Ed.* **2022**, *61*, e2022105.

[17] a) E. V. Ainsworth, C. W. J. Lockwood, G. F. White, E. T. Hwang, T. Sakai, M. A. Gross, D. J. Richardson, T. A. Clarke, L. J. C. Jeuken, E. Reisner, J. N. Butt, *ChemBioChem* **2016**, *17*, 2324; b) E. T. Hwang, K. Sheikh, K. L. Orchard, D. Hojo, V. Radu, C.-Y. Lee, E. Ainsworth, C. Lockwood, M. A. Gross, T. Adschiri, E. Reisner, J. N. Butt, L. J. C. Jeuken, *Adv. Funct. Mater.* **2015**, *25*, 2308; c) E. T. Hwang, K. L. Orchard, D. Hojo, J. Beton, C. W. J. Lockwood, T. Adschiri, J. N. Butt, E. Reisner, L. J. C. Jeuken, *ChemElectroChem* **2017**, *4*, 1959; d) T. A. Clarke, M. J. Edwards, A. J. Gates, A. Hall, G. F. White, J. Bradley, C. L. Reardon, L. Shi, A. S. Beliaev, M. J. Marshall, Z. Wang, N. J. Watmough, J. K. Fredrickson, J. M. Zachara, J. N. Butt, D. J. Richardson, *Proc. Natl. Acad. Sci. USA* **2011**, *108*, 9384.

[18] a) J. H. van Wonderen, K. Adamczyk, X. Wu, X. Jiang, S. E. H. Piper, C. R. Hall, M. J. Edwards, T. A. Clarke, H. Zhang, L. J. C. Jeuken, I. V. Sazanovich, M. Towrie, J. Blumberger, S. R. Meech, J. N. Butt, *Proc. Natl. Acad. Sci. USA* **2021**, *118*, e2107939118; b) J. H. van Wonderen, C. R. Hall, X. Jiang, K. Adamczyk, A. Carof, I. Heisler, S. E. H. Piper, T. A. Clarke, N. J. Watmough, I. V. Sazanovich, M. Towrie, S. R. Meech, J. Blumberger, J. N. Butt, *J. Am. Chem. Soc.* **2019**, *141*, 15190; c) J. H. van Wonderen, D. Li, S. E. H. Piper, C. Y. Lau, L. P. Jenner, C. R. Hall, T. A. Clarke, N. J. Watmough, J. N. Butt, *ChemBioChem* **2018**, *19*, 2206.

[19] a) X. Wang, Y. Feng, P. Dong, J. Huang, *Front. Chem.* **2019**, *7*, 671; b) M. L. Liu, B. B. Chen, C. M. Li, C. Z. Huang, *Green Chem.* **2019**, *21*, 449; c) M. Semeniuk, Z. Yi, V. Poursorkhabi, J. Tjong, S. Jaffer, Z.-H. Lu, M. Sain, *ACS Nano* **2019**, *13*, 6224; d) M. Tuerhong, Y. Xu, X.-B. Yin, *Chin. J. Anal. Chem.* **2017**, *45*, 139; e) G. A. M. Hutton, B. C. M. Martindale, E. Reisner, *Chem. Soc. Rev.* **2017**, *46*, 6111.

[20] C. Rao, S. Khan, N. C. Verma, C. K. Nandi, *ChemBioChem* **2017**, *18*, 2385.

[21] a) B. C. M. Martindale, G. A. M. Hutton, C. A. Caputo, E. Reisner, *J. Am. Chem. Soc.* **2015**, *137*, 6018; b) B. C. M. Martindale, G. A. M. Hutton, C. A. Caputo, S. Prantl, R. Godin, J. R. Durrant, E. Reisner, *Angew. Chem., Int. Ed.* **2017**, *56*, 6459.

[22] C. W. J. Lockwood, J. H. van Wonderen, M. J. Edwards, S. E. H. Piper, G. F. White, S. Newton-Payne, D. J. Richardson, T. A. Clarke, J. N. Butt, *Methods Enzymol.* **2018**, *613*, 257.

[23] K. Siriwardana, A. Wang, M. Gadogbe, W. E. Collier, N. C. Fitzkee, D. Zhang, *J. Phys. Chem. C* **2015**, *119*, 2910.

[24] M. Samsó, J.-R. Daban, S. Hansen, G. R. Jones, *Eur. J. Biochem.* **1995**, *232*, 818.

[25] T. Cedervall, I. Lynch, S. Lindman, T. Berggård, E. Thulin, H. Nilsson, K. A. Dawson, S. Linse, *Proc. Natl. Acad. Sci. USA* **2007**, *104*, 2050.

[26] M. B. Katan, *Anal. Biochem.* **1976**, *74*, 132.

[27] a) C. Gerhards, C. Schulz-Drost, V. Sgobba, D. M. Guldi, *J. Phys. Chem. B* **2008**, *112*, 14482; b) J. Sławski, R. Białek, G. Burdziński, K. Gibasiewicz, R. Worch, J. Grzyb, *J. Phys. Chem. B* **2021**, *125*, 3307; c) J. Grzyb, E. Kalwarczyk, R. Worch, *RSC Adv.* **2015**, *5*, 61973.

[28] E. H. Edwards, J. Jelušić, R. M. Kosko, K. P. McClelland, S. S. Ngarnim, W. Chiang, S. Lampa-Pastirk, T. D. Krauss, K. L. Bren, *Proc. Natl. Acad. Sci. USA* **2023**, *120*, e2206975120.

[29] C. A. Caputo, M. A. Gross, V. W. Lau, C. Cavazza, B. V. Lotsch, E. Reisner, *Angew. Chem., Int. Ed.* **2014**, *53*, 11538.

© 2023 The Authors. Advanced Functional Materials published by Wiley-VCH GmbH

16163028, 0, Downloaded from https://onlinelibrary.wiley.com/doi/10.1002/adfm.202302204 by University Of East Anglia, Wiley Online Library on [03/08/2023]. See the Terms and Conditions (https://onlinelibrary.wiley.com/terms-and-conditions) on Wiley Online Library for rules of use; OA articles are governed by the applicable Creative Commons License